

Any-to-Bokeh: One-Step Video Bokeh via Multi-Plane Image Guided Diffusion

Yang Yang^{1,2*} Siming Zheng^{2*} Jinwei Chen² Boxi Wu^{1†}
 Xiaofei He¹ Deng Cai¹ Bo Li² Peng-Tao Jiang^{2†}

¹Zhejiang University ²vivo Mobile Communication Co., Ltd
 Project Page: <https://vivocameraresearch.github.io/any2bokeh/>

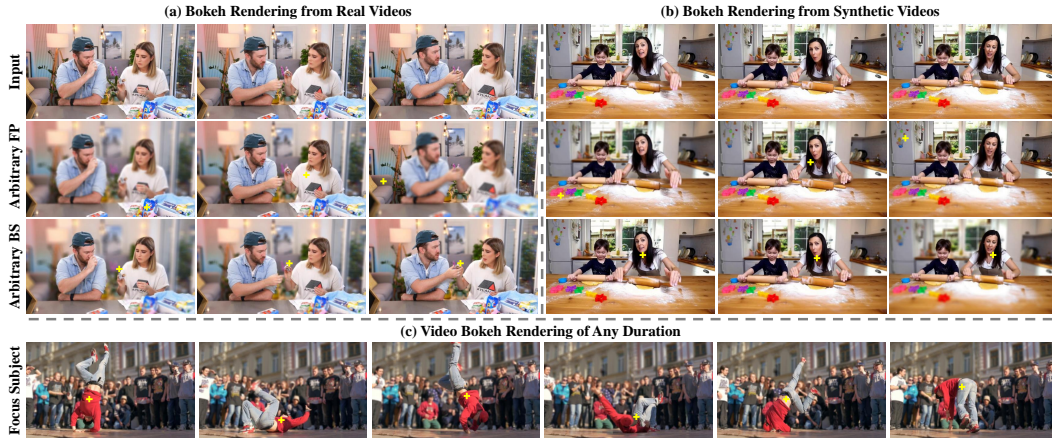


Figure 1: **Any-to-Bokeh can process videos of any length, including both real-world and synthetic videos generated by video generation models, for bokeh rendering.** The upper section demonstrates how Any-to-Bokeh enables users to customize the focal plane (FP) and adjust the blur strength (BS). The lower section highlights Any-to-Bokeh’s powerful temporal coherence in long videos. The yellow cross indicates the focal plane. Please zoom in to view the image details.

Abstract

Recent advances in diffusion based editing models have enabled realistic camera simulation and image-based bokeh, but video bokeh remains largely unexplored. Existing video editing models cannot explicitly control focus planes or adjust bokeh intensity, limiting their applicability for controllable optical effects. Moreover, naively extending image-based bokeh methods to video often results in temporal flickering and unsatisfactory edge blur transitions due to the lack of temporal modeling and generalization capability. To address these challenges, we propose a novel one-step video bokeh framework that converts arbitrary input videos into temporally coherent, depth-aware bokeh effects. Our method leverages a multi-plane image (MPI) representation constructed through a progressively widening depth sampling function, providing explicit geometric guidance for depth-dependent blur synthesis. By conditioning a single-step video diffusion model on MPI layers and utilizing the strong 3D priors from pre-trained models such as Stable Video Diffusion, our approach achieves realistic and consistent bokeh effects across diverse scenes. Additionally, we introduce a progressive training strategy to enhance temporal consistency, depth robustness, and detail preservation. Extensive experiments

*Equal contribution. Intern at vivo Mobile Communication Co., Ltd.

†Corresponding author.

demonstrate that our method produces high-quality, controllable bokeh effects and achieves state-of-the-art performance on multiple evaluation benchmarks.

1 Introduction

Recent advances in diffusion models have significantly improved camera simulation tasks, particularly in controlling geometric transformations such as lens movement, zooming, and panning [1, 2, 3, 4]. Beyond geometric aspects, recent studies have also begun to explore the rendering of synthetic bokeh in the reference image [5], aiming to simulate depth-of-field effects directly from 2D content. However, the extension of video bokeh remains largely unexplored, with no existing methods addressing the challenges of maintaining temporal coherence and structure consistency across frames. Furthermore, while current video generation models [6, 7] can occasionally produce bokeh-like effects implicitly, they lack explicit control over the focus plane. Additionally, these models are unable to freely adjust bokeh intensity, which limits their applicability in video generation scenarios that require flexible and realistic optical focus manipulation. This motivates us to develop a framework that enables controllable, temporally coherent bokeh for arbitrary input videos, filling a critical gap in the video editing research area.

While bokeh rendering has gained attention in recent years, most existing work has focused on the image-based bokeh task, where the goal is to generate shallow depth-of-field effects from a single image [8, 9, 10, 11]. In contrast, video bokeh remains in its early stages. Naively extending image-based methods [12, 13, 14, 15] to video often leads to undesirable artifacts, such as temporal flickering and inconsistent blur, due to the lack of temporal modeling and robust scene understanding. Furthermore, most current models [16, 17] are trained from scratch, without utilizing strong pre-trained priors or generalizable representations. This results in models that are overfitted to specific data distributions and overly sensitive to depth estimation errors, leading to suboptimal blur quality—especially around object boundaries.

To address these challenges, we propose a novel one-step video bokeh diffusion network that enables efficient and temporally coherent bokeh from arbitrary input videos. Our method is built upon a multi-plane image (MPI) representation [18], which provides an explicit yet compact encoding of scene geometry. Specifically, we generate MPI layers by partitioning the scene along a set of disparity intervals, constructed using a progressively widening disparity range function. This allows the model to focus on fine details in the foreground while allocating coarser attention to out-of-focus regions, enabling accurate blur transition at object boundaries. By conditioning a single-step video diffusion model on this MPI representation, the system learns to synthesize depth-aware blur effects that naturally align with subject contours, even in complex or cluttered scenes. Unlike existing methods trained from scratch, our framework leverages the strong 3D perception capabilities of large-scale pre-trained video diffusion models such as Stable Video Diffusion (SVD) [19], which are trained on diverse video data and demonstrate superior generalization and structural understanding. To further enhance temporal consistency, depth robustness, and visual detail, we adopt a three-stage progressive training strategy. In the first stage, we train the MPI spatial block and temporal block to learn bokeh rendering with accurate geometric guidance. In the second stage, we include more frames and introduce data perturbations to improve the model’s robustness and enforce temporal coherence, aiming to enhance robustness by building longer temporal sequences that better handle real-world variations. In the final stage, we incorporate a VAE-based refinement module to further enhance the fidelity of subject details and texture preservation. Together, these components form a unified framework for general-purpose video bokeh.

Extensive experiments on real-world and synthesis video benchmarks demonstrate that our method achieves superior visual quality and temporal stability compared to prior work. Our framework supports rendering from arbitrary video inputs, making high-quality bokeh video accessible and practical for a wide range of applications, including content creation, cinematic editing, and mobile post-processing. In summary, our contributions are as follows:

- We propose a one-step video bokeh framework that leverages the 3D-aware priors of large-scale pre-trained video diffusion models, departing from previous from-scratch approaches. This enables our model to generalize well to diverse videos and produce temporally coherent bokeh effects without domain-specific training.

- We introduce an MPI-guided conditioning mechanism, using a disparity-interval sampling function to construct layered scene geometry and guide spatially accurate bokeh rendering.
- We develop a progressive training strategy that significantly improves temporal consistency, depth robustness, and detail preservation, ultimately producing more realistic bokeh outputs and achieving state-of-the-art performance across multiple evaluation benchmarks.

2 Related work

2.1 Camera Simulation Diffusion Models

Reference Guidance Models. A line of work [20, 21] encodes motion cues from reference videos via LoRA [22], enabling the diffusion model to replicate specific camera behaviors observed in the training set. In contrast, MotionClone[23] proposes a training-free approach, using spatial and temporal attention modules to directly extract motion patterns from reference videos. Some works[1, 2, 3, 4] require users to draw reference points to guide the lens adjustment.

Optical Effects with Diffusion. While most prior diffusion-based camera simulation work focuses on motion modeling, recent studies have expanded to include optical effects like depth-of-field and bokeh. For instance, BokehDiffusion[5] and Generative Photography[24] propose methods to synthesize high-quality bokeh from 2D images, capturing realistic defocus effects. These works show the potential of diffusion models for simulating non-geometric camera behavior. However, they are limited to static images and lack temporal modeling, making them unsuitable for video tasks. In contrast, our work integrates optical effect simulation with pre-trained video diffusion models, enabling controllable, temporally consistent bokeh effects for arbitrary video inputs.

2.2 Computational Bokeh

Training-Free Methods. Early computational bokeh methods are model-free and rely on physically-based or image-based heuristics. Ray tracing[25, 26, 27] produces realistic defocus effects, but it requires full 3D geometry and is computationally expensive, which limits its practical applicability. Depth-based methods[28, 29] apply scattering or gathering kernels to create spatially varying blur using estimated depth. Matting-based methods [30, 31] blur the background based on foreground masks. While these methods are simple and do not require training, they often suffer from artifacts due to inaccurate depth estimation or segmentation errors, leading to unnatural blur transitions.

Learning-based Methods. Deep learning approaches improve efficiency and realism. For example, BokehMe[14] refines depth-based blur using classical methods[28] in combination with neural networks, while Multiplane Image (MPI) [32] based models [13, 18, 12] decompose the scene into layered representations for depth-aware rendering. Others adopt adaptive kernels or light field approximations [33, 34]. DeepLens [15] trained a depth estimation network using depth estimation and foreground segmentation data in order to enhance the perception of foreground edges. End-to-end models trained on paired all-in-focus and bokeh datasets [35, 10, 36] show promise but are limited by dataset biases and fixed parameter simulation. They generally lack the flexibility to control focal planes or simulate custom bokeh intensities.

While image-based bokeh synthesis is well-studied, extending it to videos is challenging. Naive frame-wise methods often introduce temporal flickering and inconsistency due to the lack of temporal modeling. Few works integrate strong pre-trained priors for video bokeh. Our work addresses this by a novel MPI-guided conditioning mechanism and leveraging pre-trained video diffusion models for consistent spatial and temporal bokeh rendering.

3 Method

An overview of our pipeline is provided in Fig. 2 (a). We propose a one-step framework for video bokeh that leverages pre-trained video priors to achieve both efficiency and enhanced visual quality. The central innovation of our approach is the MPI construction module presented in Fig. 2 (b), which effectively separates depth-aware regions and facilitates improved bokeh effect. Additionally, we introduce a progressive training strategy in Fig. 3 designed to enhance temporal consistency,

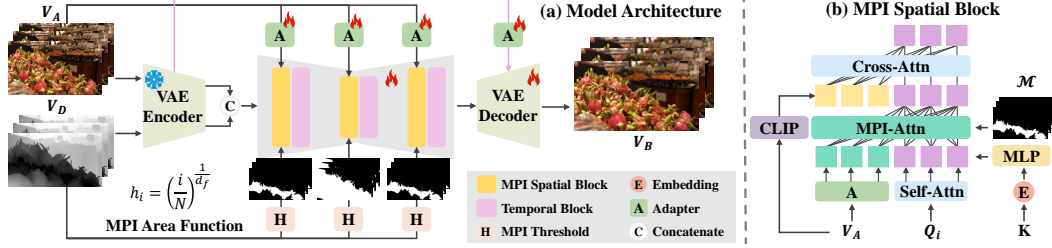


Figure 2: **Two key components of Any-to-Bokeh.** **a) One-step video bokeh model architecture:** receives input of any video and disparity relative to the focal plane to perform bokeh effect. **b) MPI spatial block:** uses the MPI mask \mathcal{M} to prompt MPI attention to focus on areas at different depths from the focal plane, guiding bokeh rendering. Additionally, high-level semantic information is injected via cross-attention to preserve more semantic structures. The user-defined blur strength K is injected through embedding.

robustness, and detail preservation. Each component of the framework is discussed in detail in the following subsections.

3.1 Preliminary

Circle of Confusion. Recent computational bokeh methods often use the circle of confusion (CoC) to estimate per-pixel blur radius [12, 13, 14]. The CoC models the size of the projected image of a point outside the focal plane. As shown in [28], the blur radius r for a pixel is defined as

$$r = K \left| \frac{1}{z} - \frac{1}{z_f} \right| = K |d - d_f|, \quad (1)$$

where K controls the overall blur strength, z denotes the depth of the pixel, and z_f represents the depth corresponding to the focus plane. We replace the depth z with the disparity (inverse depth) d to simplify the formula. In practical implementations, the CoC value determines the spatial extent over which pixel intensity is diffused. The blur kernel is typically modeled as a disk [37, 38], with its radius proportional to the CoC, enabling depth-aware rendering with soft transitions around object boundaries. Instead of manually defining the blur kernel, we feed the CoC as a condition into our model, allowing it to adaptively generate a better bokeh effect.

3.2 One-Step Video Bokeh Diffusion Model

Recent studies [39] have shown that reducing the number of diffusion steps can improve both efficiency and visual quality, especially when the model is directly conditioned on strong structural priors, such as 3D geometry [39], reference images [40, 41], or semantic masks [42]. Inspired by these advances and the demonstrated effectiveness of diffusion models in 3D perception [43, 19], we build upon the pre-trained Stable Video Diffusion (SVD) [19] framework to develop a one-step video bokeh model. Our method adopts a single-step design conditioned on MPI guidance, enabling depth-aware, temporally coherent, and controllable bokeh synthesis in video. Given a sequence of input frames and corresponding disparity maps, we encode each frame using a VAE encoder and inject MPI-derived attention masks into the diffusion process. The base model follows a U-Net architecture initialized from SVD and is conditioned on three explicit control signals: (1) a normalized disparity difference between the video disparity map and the focal plane disparity V_D , (2) a scalar blur strength parameter K , and (3) a focal plane-adapted MPI mask \mathcal{M} . These signals allow flexible control over focus positioning and bokeh intensity across the sequence.

3.3 MPI Spatial Block

As shown in Fig. 2(b), we first construct a multi-plane image (MPI) representation for each input frame and generate a focal plane-adapted MPI mask. Unlike prior works [13, 18] that discretize the scene using front-to-back layers with fixed depth values, our MPI is defined relative to the focal plane, enabling more flexible and focus-aware layer sampling. The resulting MPI mask is injected into the attention module as a geometry-aware prior to guide bokeh rendering. In parallel, high-level semantics extracted by a pre-trained CLIP image encoder are fused via cross-attention, allowing the model to preserve content structure while generating defocus effects.

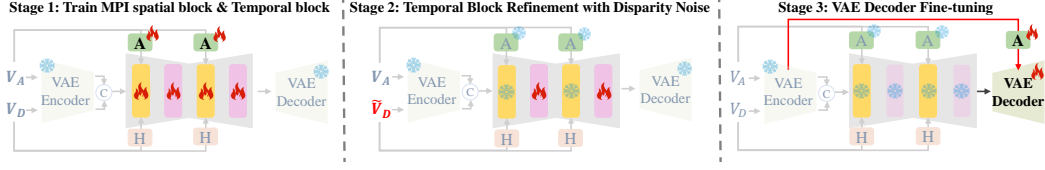


Figure 3: **Progressive Training Strategy:** Stage 1: Train the whole U-Net and adapters. Stage 2: Refine temporal block with disturbance. Stage 3: Fine-tuning VAE decoder. We desaturated the colors in the same areas.

Focal Plane-Adapted MPI Mask. To determine the disparity intervals for the MPI layers, we design a disparity-interval sampling function that gradually increases the interval width along the disparity axis. This provides finer granularity for regions near the subject’s edge and coarser sampling for background areas. As a result, the network can focus more on content near the focus plane, generating better bokeh details. We define a set of N discrete regions using an MPI area function:

$$h_i = \left(\frac{i}{N} \right)^{\frac{1}{d_f}}, i = 1, 2, \dots, N - 1. \quad (2)$$

Here, $d_f \in (0, 1]$ denotes the normalized disparity of the focal plane. As illustrated in Eq. (1), disparity changes more slowly at greater depths, and defocus effects diminish for distant regions. Based on this theory, we use $1/d_f$ as a sharpness factor, allocating finer sampling near shallow focus planes, where bokeh is more perceptible. These regions are then used to construct a focal plane-adapted MPI mask, identifying pixels whose disparity is close to the focal plane. Specifically, given a video disparity sequence d predicted by a pre-trained depth estimation network [44], we define the mask with the MPI threshold as: $\mathcal{M} = \{m_i \mid |d(m_i) - d_f| < h_i\}$.

MPI Attention. Inspired by the gated self-attention mechanism [45], we extend it by introducing our focal plane-adapted MPI mask, referred to as MPI Attention, and injecting it into the spatial attention blocks of the U-Net. Formally:

$$\hat{\mathbf{Q}} = \mathbf{Q} + \tanh(\gamma) \cdot \text{TS}(\text{Attn}([\mathbf{Q} + \Phi_M(E(K)), \Phi_A(V_A)], \bar{\mathcal{M}})), \quad (3)$$

where $\mathbf{Q} = \{Q_1, \dots, Q_i\}$ denotes the feature tokens from the current U-Net block, V_A represents visual tokens from the input video, and γ is a learnable gating parameter initialized to zero. TS is a token selection operator applied over the attended output, and $[\cdot, \cdot]$ denotes concatenation. To introduce controllable bokeh strength, we encode a user-specified control variable K representing the desired blur strength. The scalar K is first transformed via a Fourier embedding [46] $E(K)$, followed by an MLP $\Phi_M(\cdot)$, yielding a modulation term $\Phi_M(E(K))$. This term is added to each query token, enabling the attention module to condition its response based on the desired bokeh intensity. In parallel, the visual tokens V_A are projected via an adapter network $\Phi_A(\cdot)$, which consists of a lightweight MLP and maps V_A to the same dimensionality as the query tokens. To modulate attention for focus proximity, we reconstruct the mask $\bar{\mathcal{M}} = [\mathbf{1}, \mathcal{M}]$, where $\mathbf{1}$ assigns full attention weight to \mathbf{Q} . This encourages the model to attend more to focus-relevant regions. Focal plane-adapted MPI masks are injected at multiple U-Net stages: shallow layers receive the near-focal-plane mask to focus on areas with sensitive changes, while deeper layers capture masks for larger depth intervals, allowing for a broader receptive field. Bilinear interpolation is used to align mask resolutions with U-Net block input.

Semantic Injection. We extract global semantic features from the visual token V_A using the CLIP image encoder [47]. The resulting embeddings are injected into the U-Net via cross-attention, where CLIP embeddings serve as queries and visual tokens as keys and values. This enhances the network’s ability to preserve semantic structure and produce content-aware bokeh effects.

3.4 Progressive Training Strategy

As shown in Fig. 3, we approach a three-stage training strategy to improve temporal consistency, depth robustness, and fine detail preservation.

Stage 1: U-Net Fine-tuning. In the first stage, we train the MPI spatial block, temporal block, and adapters using clean data. This allows the model to quickly adapt to the video-to-video bokeh task. Training without noise encourages the network to better leverage the guidance provided by the focal

plane-adapted MPI mask, improving its ability to synthesize spatially accurate and depth-aware bokeh effects. This stage also helps the model establish initial temporal consistency across video frames.

Stage 2: Temporal Block Refinement with Disparity Noise. In the second stage, we freeze the MPI spatial block of the U-Net and train only the temporal blocks using more frames. To enhance the model’s robustness, we introduce a combination of noise perturbations specifically targeting the disparity boundaries in the focus region. First, we apply elastic transform [48] to distort the depth map locally around the focal region. Next, we inject Perlin noise [49] into these perturbed areas to simulate natural depth inconsistencies. Finally, we apply morphological dilation and erosion operations to further exaggerate the boundary transitions. This staged perturbation strategy prevents the MPI spatial blocks from being overwhelmed by both temporal modeling and complex disparity noise simultaneously. By injecting controlled disparity noise, the model learns to be less dependent on precise depth values and becomes more resilient to real-world variations in depth estimation. Additionally, training with longer temporal sequences allows the model to leverage longer temporal memory, reducing bokeh flickering caused by depth noise.

Stage 3: VAE Decoder Fine-tuning. In the final stage, we fine-tune only the VAE decoder and its adapter to recover high-frequency details that are often lost during encoding. Clean data is used in this phase to promote high-fidelity reconstruction. Inspired by prior work [50], we introduce a skip connection from the VAE encoder to the decoder by applying a simple convolution to the encoder features, enabling the decoder to reuse spatially rich representations. To preserve fine details, we use a combination of image-space L1 loss and texture loss $\mathcal{L} = \mathcal{L}_1(\hat{V}_B, V_B) + \mathcal{L}_t$, where \hat{V}_B is the prediction result V_B is the ground truth. The texture loss is computed by comparing the gradients of the predicted and ground truth images along the horizontal and vertical directions using the Sobel operator. Specifically, the loss is defined as the squared sum of the gradient differences:

$$\mathcal{L}_t = \sum_{x,y} \left((\nabla_x \hat{V}_B(x,y) - \nabla_x V_B(x,y))^2 + (\nabla_y \hat{V}_B(x,y) - \nabla_y V_B(x,y))^2 \right), \quad (4)$$

which helps the model better capture fine details like edges and textures, improving the bokeh effect.

3.5 Weighted Overlap Inference Strategy

To enhance the model’s capability for inference on long videos and to ensure seamless temporal consistency across video segments, we propose a weighted overlapping inference strategy (WOIS). This method effectively tackles the critical issue of boundary inconsistencies commonly introduced by naive sequence splitting, which typically degrades visual quality. Our strategy involves dividing the input video into P overlapping segments denoted as $\hat{V}_B^0, \hat{V}_B^1, \dots, \hat{V}_B^P$, each consisting of $2L$ frames, with adjacent segments overlapping by exactly L frames. For the j -th frame in the i -th overlapping segment, denoted by $\hat{V}_B^i[j]$, we obtain the fused result $\tilde{V}_B^i[j]$ through a weighted combination:

$$\tilde{V}_B^i[j] = \gamma_j \hat{V}_B^i[j] + (1 - \gamma_j) \hat{V}_B^{i+1}[j], \quad i \in 1, 2, \dots, P, \quad (5)$$

where the weighting factor γ_j employs a cosine-based function defined as $\gamma_j = \frac{1}{2} (1 + \cos(\frac{\pi j}{L}))$ to ensure smooth and visually coherent transitions between consecutive video segments.

4 Experiments

4.1 Implementation Details

Dataset. Currently, no paired datasets for the all-in-focus and bokeh videos. Existing computational bokeh datasets [35, 10, 36] primarily consist of image pairs but lack temporal consistency, and previous video-based works [16] often omit foreground motion. To address this, we build upon prior work [37] and adopt a synthetic approach to generate paired all-in-focus and bokeh video sequences. For accurate foreground extraction, we use objects from the video matting dataset [51], isolating them using the alpha channel for precise segmentation. To augment the dataset, we also incorporate the image matting dataset [52] and collect 1,300 background images from the intern dataset and background dataset [51]. In each video, we randomly select background and foreground clips, simulating real-world camera adjustments such as focal plane and aperture changes. The foreground objects are moved along random 3D trajectories, each containing 25 frames. All videos

| Method | FD↓ | RM↓ | VFID-I↓ | FVD↓ | SSIM↑ | PSNR↑ | Time↓ |
|---------------------|--------------|--------------|--------------|--------------|--------------|---------------|--------------|
| DeepLens [15] | 1.162 | 0.030 | 16.042 | 125.338 | 0.819 | 24.574 | 0.226 |
| BokehMe [14] | 0.536 | 0.013 | 8.633 | 39.102 | 0.936 | 27.992 | 0.103 |
| Dr.Bokeh [12] | 0.522 | 0.011 | 6.097 | 32.710 | 0.950 | 31.273 | 2.729 |
| MPIB [13] | 0.481 | 0.011 | 5.444 | 35.766 | 0.950 | 31.390 | 0.521 |
| Any-to-Bokeh | 0.431 | 0.007 | 1.479 | 9.005 | 0.974 | 38.899 | 0.363 |

Table 1: **Quantitative comparison of Any-to-Bokeh.** The best metric scores in each column are marked in **bold** for clarity. “↓” or “↑” indicate lower or higher values are better.

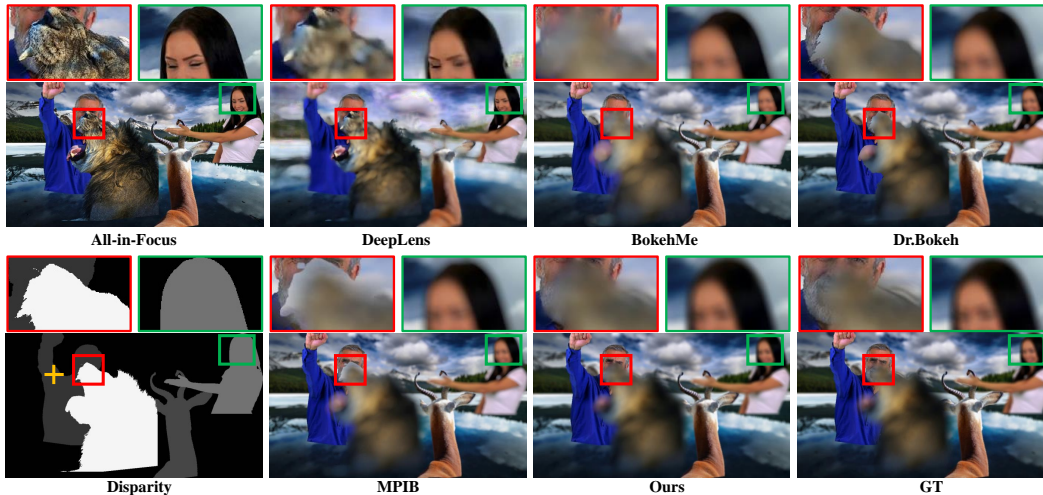


Figure 4: **Qualitative results on the synthetic test dataset.** The focal plane is marked by a yellow cross on the disparity map. To highlight the differences, we zoom in on the red and green regions.

in the dataset have a resolution of 1024×576 pixels. Using a ray-tracing-based method [13], we generate accurate bokeh effects, ensuring temporal coherence across frames. To evaluate model performance, we synthesize a test set of 200 videos with varying bokeh strength and focus planes.

Training and Inference. In this work, we use SVD [19] as our base model. During training, the process is divided into three stages: Stage 1: We train using 4-frame video sequences with the Adam optimizer at a learning rate of $1e-5$. Stage 2: We train with 8-frame video sequences, using a learning rate of $5e-6$ and a depth perturbation probability of 0.5. Stage 3: We fine-tune the VAE decoder using the same learning rate as in Stage 2. For all stages, the video resolution is set to 1024×576 with a batch size of 1, and training is performed across 4 Nvidia H800 GPUs. During inference, we use the weighted overlap inference strategy where long videos are divided into clips of 8 frames, with each clip having a 4-frame overlap.

Metrics. For evaluation, we report the following metrics: PSNR and SSIM[53] for image fidelity. For video quality, we use VFID [54] with features from I3D[55] (denoted VFID-I) and FVD[56]. To assess temporal consistency, we use the relation metric[16] (denoted as RM) to compute the pixel-wise difference between adjacent frames, and the flow difference between predicted and ground truth frames, both estimated with RAFT [57] (referred to as FD).

4.2 Results on Test Dataset

To verify the performance of our proposed method, we compare it with four existing computational bokeh methods: DeepLens [15], BokehMe [14], Dr.Bokeh [12], and MPIB [13]. Specifically, to compare with traditional MPI-based bokeh methods, MPIB and Dr.Bokeh use the conventional approach, which differs from the one introduced in Sec. 3.3. To our knowledge, there is only one related work [16] on video bokeh, and since it is not open-source, we cannot compare it.

Quantitative Results. As shown in Tab. 1, our method consistently outperforms all other approaches across all metrics. Specifically, Any-to-Bokeh achieves the lowest flow difference (FD) and the best relation metric (RM), demonstrating superior temporal consistency. This improvement underscores

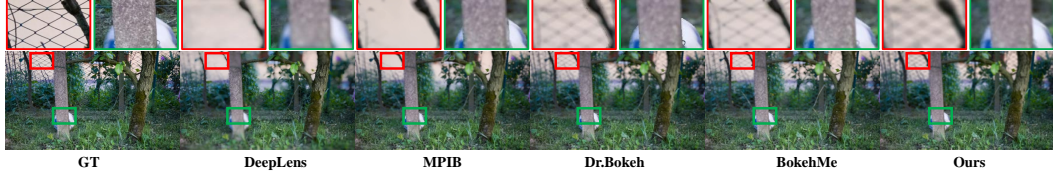


Figure 5: **Qualitative results on the real video.** The focal plane is located on the football. For each method, we only present the middle frame. Please zoom in to view the image details.

the effectiveness of the SVD pre-trained prior in reducing flickering and inconsistent blur, resulting in a temporally consistent bokeh effect. Additionally, our method significantly outperforms the baselines in video quality, achieving the lowest VFID-I and FVD, highlighting its ability to generate high-quality, temporally coherent bokeh effects. In terms of image fidelity, Any-to-Bokeh also achieves the highest SSIM and PSNR, further confirming its superior performance in bokeh effects. Furthermore, compared with the traditional MPI method, we measured the time required for inference on a single frame and found that our approach has an efficiency advantage.

Qualitative Results. To further highlight the visual advantages of our approach, we present examples in Fig. 4. Despite the guidance of the precise disparity map in the synthetic test set, the baseline methods exhibit varying degrees of bleeding (highlighted in red boxes), and the girl’s hair shows unsatisfactory deformation (highlighted in green boxes). Specifically, MPIB and Dr.Bokeh, both based on traditional MPI methods, produce discordant edges (highlighted in the red box). This further demonstrates the effectiveness of our approach. Additionally, to verify the effectiveness of our model in real-life scenarios, we tested our approach on a real video dataset [58]. As shown in Fig. 5, our method preserves better details and generates more natural bokeh effects (highlighted in the red box). Furthermore, the effect in the green box shows that our method maintains smoother object edges and reduces jaggedness at the edges during bokeh rendering. More results can be found in the appendix.

Bokeh Rendering Results on Real Video. Generating high-quality, temporally consistent bokeh on real-world videos is more challenging due to complex motion and camera shake. We test on the DAVIS [58] dataset, using Video Depth Anything [44] for disparity prediction. By leveraging foreground masks, we obtain the focal plane. As shown in Fig. 6, our method generates bokeh effects that follow optical principles and maintain strong temporal consistency. We also conducted a user study on real-world videos to better evaluate different methods from a subjective perspective. We randomly selected 20 videos from the DAVIS dataset and rendered them using various methods. Each participant viewed two videos at a time: one generated by our method and one from a randomly selected baseline (DeepLens [15], MPIB [13], BokehMe [14], or Dr.Bokeh [12]). The videos were presented in random order. Participants were asked to choose the method that produced the most aesthetically pleasing bokeh effect based on their personal preference. If they found it difficult to decide, they were allowed to skip making a selection. The user study involved 24 participants and provided 480 ratings across these video sets. The results in Tab. 2 indicate that our method was preferred over the others, demonstrating a higher human preference for the bokeh effects generated by our approach.

| Baseline | Preference |
|-------------------|---------------|
| Ours vs. DeepLens | 90.1% / 9.9% |
| Ours vs. BokehMe | 77.8% / 22.2% |
| Ours vs. MPIB | 67.5% / 32.5% |
| Ours vs. Dr.Bokeh | 60.3% / 39.7% |

Table 2: Results on human preference.

4.3 Ablation Studies

We evaluate the effectiveness of each component in the Any-to-Bokeh framework in Tab. 3 and assess the VAE’s contribution to video detail quality in Tab. 4.

MPI Block Ablation. The last three rows in the upper part show the ablation results of the MPI block. First, we remove the MPI module and use the original attention block, adding the blur strength (K) embedding directly to the original SVD embedding. From the VFID and FVD metrics, we observe that our model benefits significantly from the MPI blocks, leading to better video quality. Additionally, the MPI block greatly enhances temporal consistency and single-frame quality, which are crucial for the bokeh rendering task. Additionally, we investigate the impact of the SVD pre-trained prior (PR) on the model. As mentioned in the Sec. 3.2, SVD provides strong 3D prior knowledge, and its

| MPI | PR | WOIS | TR | FD↓ | RM↓ | VFID-I↓ | FVD↓ | SSIM↑ | PSNR↑ |
|-----|----|------|----|-------|-------|---------|--------|-------|--------|
| ✓ | ✓ | ✓ | ✓ | 0.517 | 0.013 | 3.865 | 18.922 | 0.907 | 32.250 |
| ✓ | ✓ | ✓ | | 0.540 | 0.013 | 4.209 | 20.743 | 0.905 | 32.035 |
| ✓ | ✓ | | | 0.551 | 0.013 | 4.521 | 21.941 | 0.905 | 31.936 |
| | ✓ | | | 0.568 | 0.014 | 4.714 | 22.556 | 0.901 | 31.575 |
| ✓ | | | | 0.586 | 0.014 | 4.537 | 27.743 | 0.893 | 30.988 |
| ✓ | ✓ | ✓ | ✓ | 0.531 | 0.013 | 3.880 | 19.648 | 0.906 | 32.182 |
| ✓ | ✓ | ✓ | | 0.566 | 0.014 | 4.442 | 22.452 | 0.904 | 31.890 |

Table 3: **Ablation study of Any-to-Bokeh.** The last two lines compare the contribution of TR to the robustness against inaccurate disparity. Subsequent lines show the enhancements of each module. “MPI”: MPI spacial block. “PR”: SVD pre-trained prior. “WOIS”: weighted overlap inference strategy. “TR”: temporal block refinement.



Figure 6: Visualization of generated bokeh effects on real videos. Please zoom in to see the details.

incorporation leads to improvements across all metrics. This is especially evident in the FVD score, where the contribution to video quality is substantial.

Effectiveness of Weighted Overlap Inference Strategy (WOIS). By incorporating WOIS, our model achieves improved temporal consistency, with the flow difference (FD) decreasing from 0.551 to 0.540. Additionally, higher FVD and VFID scores indicate enhanced video quality. Furthermore, the PSNR also shows an increase, reflecting improved single-frame fidelity.

Effectiveness of Progressive Training Strategy. We begin the ablation study by evaluating the full model. In the second row, we remove the temporal block refinement (TR) from stage 2, resulting in a decrease in temporal consistency (FD: 0.517 vs. 0.540). This highlights the importance of temporal block refinement in maintaining temporal coherence across video frames. As shown in Tab. 4, we alleviated the loss of high-frequency information by fine-tuning the VAE, which effectively improves both single-frame consistency and overall video quality.

| VF | FVD↓ | SSIM↑ | PSNR↑ |
|----|--------|-------|--------|
| ✓ | 9.005 | 0.974 | 38.899 |
| | 18.922 | 0.907 | 32.250 |

Table 4: Ablation study on VAE fine-tuning. VAE fine-tuning effectively enhances video quality.

Ablation Study on Robustness. To test the contribution of TR to robustness, we introduce perturbations to the disparity in the test dataset using elastic transform [48], Gaussian blur, and morphological transformations. As shown in the last two rows in Tab. 3, TR leads to improvements across all metrics, with particularly noticeable gains in temporal consistency (FD and RM) and video quality (VFID-I and FVD). These results demonstrate that training the temporal blocks with noisy data during the TR stage effectively enhances the model’s robustness.

5 Conclusions

In this work, we propose a novel one-step video bokeh framework that enables controllable and temporally consistent bokeh effects from arbitrary video inputs. By leveraging the 3D-aware priors

of pre-trained video diffusion models and incorporating an MPI-guided conditioning mechanism, our method achieves higher-quality and more generalized bokeh effects. Additionally, we introduce a progressive training strategy that enhances robustness and detail preservation, significantly improving the quality of bokeh effects. We hope our findings inspire further exploration of optical phenomena in editing models, driving advancements in their application to content creation and visual effects. By better understanding these phenomena, we aim to enhance the realism and flexibility of future editing models, enabling more creative possibilities for the industry.

References

- [1] Yao Teng, Enze Xie, Yue Wu, Haoyu Han, Zhenguo Li, and Xihui Liu. Drag-a-video: Non-rigid video editing with point-based interaction. *arXiv preprint arXiv:2312.02936*, 2023.
- [2] Yujun Shi, Chuhui Xue, Jun Hao Liew, Jiachun Pan, Hanshu Yan, Wenqing Zhang, Vincent YF Tan, and Song Bai. Dragdiffusion: Harnessing diffusion models for interactive point-based image editing. In *Proceedings of the IEEE/CVF Conference on Computer Vision and Pattern Recognition*, pages 8839–8849, 2024.
- [3] Weijia Wu, Zhuang Li, Yuchao Gu, Rui Zhao, Yefei He, David Junhao Zhang, Mike Zheng Shou, Yan Li, Tingting Gao, and Di Zhang. Draganything: Motion control for anything using entity representation. In *European Conference on Computer Vision*, pages 331–348. Springer, 2024.
- [4] Shengming Yin, Chenfei Wu, Jian Liang, Jie Shi, Houqiang Li, Gong Ming, and Nan Duan. Dragnuwa: Fine-grained control in video generation by integrating text, image, and trajectory. *arXiv preprint arXiv:2308.08089*, 2023.
- [5] Armando Fortes, Tianyi Wei, Shangchen Zhou, and Xingang Pan. Bokeh diffusion: Defocus blur control in text-to-image diffusion models. *arXiv preprint arXiv:2503.08434*, 2025.
- [6] Ang Wang, Baole Ai, Bin Wen, Chaojie Mao, Chen-Wei Xie, Di Chen, Feiwu Yu, Haiming Zhao, Jianxiao Yang, Jianyuan Zeng, Jiayu Wang, Jingfeng Zhang, Jingren Zhou, Jinkai Wang, Jixuan Chen, Kai Zhu, Kang Zhao, Keyu Yan, Lianghua Huang, Mengyang Feng, Ningyi Zhang, Pandeng Li, Pingyu Wu, Ruihang Chu, Ruili Feng, Shiwei Zhang, Siyang Sun, Tao Fang, Tianxing Wang, Tianyi Gui, Tingyu Weng, Tong Shen, Wei Lin, Wei Wang, Wei Wang, Wenmeng Zhou, Wenten Wang, Wenting Shen, Wenyuan Yu, Xianzhong Shi, Xiaoming Huang, Xin Xu, Yan Kou, Yangyu Lv, Yifei Li, Yijing Liu, Yiming Wang, Yingya Zhang, Yitong Huang, Yong Li, You Wu, Yu Liu, Yulin Pan, Yun Zheng, Yuntao Hong, Yupeng Shi, Yutong Feng, Zeyinzi Jiang, Zhen Han, Zhi-Fan Wu, and Ziyu Liu. Wan: Open and advanced large-scale video generative models. *arXiv preprint arXiv:2503.20314*, 2025.
- [7] Zhuoyi Yang, Jiayan Teng, Wendi Zheng, Ming Ding, Shiyu Huang, Jiazheng Xu, Yuanming Yang, Wenyi Hong, Xiaohan Zhang, Guanyu Feng, et al. Cogvideox: Text-to-video diffusion models with an expert transformer. *arXiv preprint arXiv:2408.06072*, 2024.
- [8] Pratul P Srinivasan, Rahul Garg, Neal Wadhwa, Ren Ng, and Jonathan T Barron. Aperture supervision for monocular depth estimation. In *Proceedings of the IEEE Conference on Computer Vision and Pattern Recognition*, pages 6393–6401, 2018.
- [9] Lei Xiao, Anton Kaplanyan, Alexander Fix, Matt Chapman, and Douglas Lanman. Deepfocus: Learned image synthesis for computational display. In *ACM SIGGRAPH 2018 Talks*, pages 1–2. 2018.
- [10] Tim Seizinger, Florin-Alexandru Vasluianu, Marcos V Conde, and Radu Timofte. Bokehlicious: Photorealistic bokeh rendering with controllable apertures. *arXiv preprint arXiv:2503.16067*, 2025.
- [11] Tim Seizinger, Marcos V Conde, Manuel Kolmet, Tom E Bishop, and Radu Timofte. Efficient multi-lens bokeh effect rendering and transformation. In *Proceedings of the IEEE/CVF Conference on Computer Vision and Pattern Recognition*, pages 1633–1642, 2023.

- [12] Yichen Sheng, Zixun Yu, Lu Ling, Zhiwen Cao, Xuaner Zhang, Xin Lu, Ke Xian, Haiting Lin, and Bedrich Benes. Dr. bokeh: differentiable occlusion-aware bokeh rendering. In *Proceedings of the IEEE/CVF Conference on Computer Vision and Pattern Recognition*, pages 4515–4525, 2024.
- [13] Juewen Peng, Jianming Zhang, Xianrui Luo, Hao Lu, Ke Xian, and Zhiguo Cao. Mpib: An mpi-based bokeh rendering framework for realistic partial occlusion effects. In *European Conference on Computer Vision*, pages 590–607. Springer, 2022.
- [14] Juewen Peng, Zhiguo Cao, Xianrui Luo, Hao Lu, Ke Xian, and Jianming Zhang. Bokehme: When neural rendering meets classical rendering. In *Proceedings of the IEEE/CVF conference on computer vision and pattern recognition*, pages 16283–16292, 2022.
- [15] Wang Lijun, Shen Xiaohui, Zhang Jianming, Wang Oliver, Lin Zhe, Hsieh Chih-Yao, Kong Sarah, and Lu Huchuan. Deeplens: Shallow depth of field from a single image. *ACM Trans. Graph. (Proc. SIGGRAPH Asia)*, 37(6):6:1–6:11, 2018.
- [16] Yawen Luo, Min Shi, Liao Shen, Yachuan Huang, Zixuan Ye, Juewen Peng, and Zhiguo Cao. Video bokeh rendering: Make casual videography cinematic. In *ACM Multimedia 2024*, 2024.
- [17] Xuaner Zhang, Kevin Matzen, Vivien Nguyen, Dillon Yao, You Zhang, and Ren Ng. Synthetic defocus and look-ahead autofocus for casual videography. *ACM Transactions on Graphics (TOG)*, 38(4):1–16, 2019.
- [18] Benjamin Busam, Matthieu Hog, Steven McDonagh, and Gregory Slabaugh. Sterefo: Efficient image refocusing with stereo vision. In *Proceedings of the IEEE/CVF international conference on computer vision workshops*, pages 0–0, 2019.
- [19] Andreas Blattmann, Tim Dockhorn, Sumith Kulal, Daniel Mendelevitch, Maciej Kilian, Dominik Lorenz, Yam Levi, Zion English, Vikram Voleti, Adam Letts, et al. Stable video diffusion: Scaling latent video diffusion models to large datasets. *arXiv preprint arXiv:2311.15127*, 2023.
- [20] Rui Zhao, Yuchao Gu, Jay Zhangjie Wu, David Junhao Zhang, Jia-Wei Liu, Weijia Wu, Jussi Keppo, and Mike Zheng Shou. Motiondirector: Motion customization of text-to-video diffusion models. In *European Conference on Computer Vision*, pages 273–290. Springer, 2024.
- [21] Yuwei Guo, Ceyuan Yang, Anyi Rao, Zhengyang Liang, Yaohui Wang, Yu Qiao, Maneesh Agrawala, Dahua Lin, and Bo Dai. Animatediff: Animate your personalized text-to-image diffusion models without specific tuning. *International Conference on Learning Representations*, 2024.
- [22] Edward J Hu, Yelong Shen, Phillip Wallis, Zeyuan Allen-Zhu, Yanzhi Li, Shean Wang, Lu Wang, and Weizhu Chen. LoRA: Low-rank adaptation of large language models. In *International Conference on Learning Representations*, 2022.
- [23] Pengyang Ling, Jiazi Bu, Pan Zhang, Xiaoyi Dong, Yuhang Zang, Tong Wu, Huaian Chen, Jiaqi Wang, and Yi Jin. Motionclone: Training-free motion cloning for controllable video generation. In *The Thirteenth International Conference on Learning Representations*, 2025.
- [24] Yu Yuan, Xijun Wang, Yichen Sheng, Prateek Chennuri, Xingguang Zhang, and Stanley Chan. Generative photography: Scene-consistent camera control for realistic text-to-image synthesis. *CVPR*, 2025.
- [25] Matt Pharr, Wenzel Jakob, and Greg Humphreys. *Physically based rendering: From theory to implementation*. MIT Press, 2023.
- [26] Michael Potmesil and Indranil Chakravarty. A lens and aperture camera model for synthetic image generation. *ACM SIGGRAPH Computer Graphics*, 15(3):297–305, 1981.
- [27] Tomas Akenine-Moller, Eric Haines, and Naty Hoffman. *Real-time rendering*. AK Peters/crc Press, 2019.

- [28] Neal Wadhwa, Rahul Garg, David E Jacobs, Bryan E Feldman, Nori Kanazawa, Robert Carroll, Yair Movshovitz-Attias, Jonathan T Barron, Yael Pritch, and Marc Levoy. Synthetic depth-of-field with a single-camera mobile phone. *ACM Transactions on Graphics (ToG)*, 37(4):1–13, 2018.
- [29] Yang Yang, Haiting Lin, Zhan Yu, Sylvain Paris, and Jingyi Yu. Virtual dslr: High quality dynamic depth-of-field synthesis on mobile platforms. *Electronic Imaging*, 28:1–9, 2016.
- [30] Xiaoyong Shen, Aaron Hertzmann, Jiaya Jia, Sylvain Paris, Brian Price, Eli Shechtman, and Ian Sachs. Automatic portrait segmentation for image stylization. In *Computer Graphics Forum*, volume 35, pages 93–102. Wiley Online Library, 2016.
- [31] Xiaoyong Shen, Xin Tao, Hongyun Gao, Chao Zhou, and Jiaya Jia. Deep automatic portrait matting. In *Computer Vision–ECCV 2016: 14th European Conference, Amsterdam, The Netherlands, October 11–14, 2016, Proceedings, Part I 14*, pages 92–107. Springer, 2016.
- [32] Tinghui Zhou, Richard Tucker, John Flynn, Graham Fyffe, and Noah Snavely. Stereo magnification: Learning view synthesis using multiplane images. *arXiv preprint arXiv:1805.09817*, 2018.
- [33] Pratul P. Srinivasan, Rahul Garg, Neal Wadhwa, Ren Ng, and Jonathan T. Barron. Aperture supervision for monocular depth estimation. In *Proceedings of the IEEE Conference on Computer Vision and Pattern Recognition (CVPR)*, June 2018.
- [34] Takuhiro Kaneko. Unsupervised learning of depth and depth-of-field effect from natural images with aperture rendering generative adversarial networks. In *Proceedings of the IEEE/CVF Conference on Computer Vision and Pattern Recognition*, pages 15679–15688, 2021.
- [35] Andrey Ignatov, Jagruti Patel, and Radu Timofte. Rendering natural camera bokeh effect with deep learning. In *Proceedings of the IEEE/CVF Conference on Computer Vision and Pattern Recognition Workshops*, pages 418–419, 2020.
- [36] Saikat Dutta, Sourya Dipta Das, Nisarg A Shah, and Anil Kumar Tiwari. Stacked deep multi-scale hierarchical network for fast bokeh effect rendering from a single image. In *Proceedings of the IEEE/CVF Conference on Computer Vision and Pattern Recognition*, pages 2398–2407, 2021.
- [37] Juewen Peng, Zhiguo Cao, Xianrui Luo, Ke Xian, Wenfeng Tang, Jianming Zhang, and Guosheng Lin. Bokehme++: Harmonious fusion of classical and neural rendering for versatile bokeh creation. *IEEE Transactions on Pattern Analysis and Machine Intelligence*, 47(3):1530–1547, 2025.
- [38] Xianrui Luo, Juewen Peng, Ke Xian, Zijin Wu, and Zhiguo Cao. Bokeh rendering from defocus estimation. In *European Conference on Computer Vision*, pages 245–261. Springer, 2020.
- [39] Guangkai Xu, Yongtao Ge, Mingyu Liu, Chengxiang Fan, Kangyang Xie, Zhiyue Zhao, Hao Chen, and Chunhua Shen. What matters when repurposing diffusion models for general dense perception tasks? *arXiv preprint arXiv:2403.06090*, 2024.
- [40] Rongyuan Wu, Lingchen Sun, Zhiyuan Ma, and Lei Zhang. One-step effective diffusion network for real-world image super-resolution. In *The Thirty-eighth Annual Conference on Neural Information Processing Systems*, 2024.
- [41] Shiyue Yan, Xiaoshi Qiu, Qingmin Liao, Jing-Hao Xue, and Shaojun Liu. Reschedule diffusion-based bokeh rendering. In *IJCAI International Joint Conference on Artificial Intelligence*, pages 1543–1551. IJCAI, 2024.
- [42] Muzhi Zhu, Yang Liu, Zekai Luo, Chenchen Jing, Hao Chen, Guangkai Xu, Xinlong Wang, and Chunhua Shen. Unleashing the potential of the diffusion model in few-shot semantic segmentation. *arXiv preprint arXiv:2410.02369*, 2024.
- [43] Vikram Voleti, Chun-Han Yao, Mark Boss, Adam Letts, David Pankratz, Dmitry Tochilkin, Christian Laforte, Robin Rombach, and Varun Jampani. Sv3d: Novel multi-view synthesis and 3d generation from a single image using latent video diffusion. In *European Conference on Computer Vision*, pages 439–457. Springer, 2024.

- [44] Sili Chen, Hengkai Guo, Shengnan Zhu, Feihu Zhang, Zilong Huang, Jiashi Feng, and Bingyi Kang. Video depth anything: Consistent depth estimation for super-long videos. *arXiv preprint arXiv:2501.12375*, 2025.
- [45] Yuheng Li, Haotian Liu, Qingyang Wu, Fangzhou Mu, Jianwei Yang, Jianfeng Gao, Chunyuan Li, and Yong Jae Lee. Gligen: Open-set grounded text-to-image generation. *CVPR*, 2023.
- [46] Ben Mildenhall, Pratul P Srinivasan, Matthew Tancik, Jonathan T Barron, Ravi Ramamoorthi, and Ren Ng. Nerf: Representing scenes as neural radiance fields for view synthesis. *Communications of the ACM*, 65(1):99–106, 2021.
- [47] Alec Radford, Jong Wook Kim, Chris Hallacy, Aditya Ramesh, Gabriel Goh, Sandhini Agarwal, Girish Sastry, Amanda Askell, Pamela Mishkin, Jack Clark, et al. Learning transferable visual models from natural language supervision. In *International conference on machine learning*, pages 8748–8763. PmLR, 2021.
- [48] Alexander Buslaev, Vladimir I. Iglovikov, Eugene Khvedchenya, Alex Parinov, Mikhail Druzhinin, and Alexandr A. Kalinin. Albumentations: Fast and flexible image augmentations. *Information*, 11(2), 2020.
- [49] Ken Perlin. An image synthesizer. *ACM Siggraph Computer Graphics*, 19(3):287–296, 1985.
- [50] Gaurav Parmar, Taesung Park, Srinivasa Narasimhan, and Jun-Yan Zhu. One-step image translation with text-to-image models. *arXiv preprint arXiv:2403.12036*, 2024.
- [51] Shanchuan Lin, Andrey Ryabtsev, Soumyadip Sengupta, Brian L Curless, Steven M Seitz, and Ira Kemelmacher-Shlizerman. Real-time high-resolution background matting. In *Proceedings of the IEEE/CVF Conference on Computer Vision and Pattern Recognition*, pages 8762–8771, 2021.
- [52] Jizhi Li, Jing Zhang, Stephen J Maybank, and Dacheng Tao. Bridging composite and real: towards end-to-end deep image matting. *International Journal of Computer Vision*, 130(2):246–266, 2022.
- [53] Zhou Wang, Alan C Bovik, Hamid R Sheikh, and Eero P Simoncelli. Image quality assessment: from error visibility to structural similarity. *IEEE transactions on image processing*, 13(4):600–612, 2004.
- [54] Ting-Chun Wang, Ming-Yu Liu, Jun-Yan Zhu, Guilin Liu, Andrew Tao, Jan Kautz, and Bryan Catanzaro. Video-to-video synthesis. In *Proceedings of the 32nd International Conference on Neural Information Processing Systems*, pages 1152–1164, 2018.
- [55] Joao Carreira and Andrew Zisserman. Quo vadis, action recognition? a new model and the kinetics dataset. In *proceedings of the IEEE Conference on Computer Vision and Pattern Recognition*, pages 6299–6308, 2017.
- [56] Songwei Ge, Aniruddha Mahapatra, Gaurav Parmar, Jun-Yan Zhu, and Jia-Bin Huang. On the content bias in fr chet video distance. In *Proceedings of the IEEE/CVF Conference on Computer Vision and Pattern Recognition (CVPR)*, 2024.
- [57] Zachary Teed and Jia Deng. Raft: Recurrent all-pairs field transforms for optical flow. In *Computer Vision–ECCV 2020: 16th European Conference, Glasgow, UK, August 23–28, 2020, Proceedings, Part II 16*, pages 402–419. Springer, 2020.
- [58] Federico Perazzi, Jordi Pont-Tuset, Brian McWilliams, Luc Van Gool, Markus Gross, and Alexander Sorkine-Hornung. A benchmark dataset and evaluation methodology for video object segmentation. In *The IEEE Conference on Computer Vision and Pattern Recognition (CVPR)*, 2016.



Figure 7: Example of synthetic datasets, we randomly define the focal plane, the position of each foreground, and the blur intensity.



Figure 8: The user study interface, where they were asked to select their preferred videos.

A The Details of Dataset

As mentioned on Sec. 4.1, we use objects from the video matting dataset [51] and image matting dataset [52] and collect 1,300 background images from the intern dataset and background dataset [51]. Following MPIB [13], we use a ray-tracing-based method to generate accurate bokeh effects. Specifically, we assume that the disparities of all images are planar, with their size and position randomly determined. The disparity map d is then set as a plane equation of pixel coordinates (x, y)

$$d = \frac{1 - ax - by}{c}, \quad (6)$$

where a , b , and c are parameters that define the spatial depth relationship between pixels. For each pixel, we sample multiple rays passing through the lens, find the intersection of each ray with the scene, and project this intersection onto the sensor plane to obtain the final render results. As shown in Fig. 7, for each video, we randomly select background and foreground clips, as well as the focal plane and aperture. The foreground objects are moved along random 3D trajectories, with movement in six dimensions: forward and backward, left and right, up and down. Each video contains 25 frames, and all videos in the dataset have a resolution of 1024×576 pixels. To evaluate model performance, we use the same approach to synthesize a test set of 200 videos.

B User Study Details

Given the subjective nature of perceiving video bokeh rendering results, and the absence of ground truth (GT) data for video bokeh, we conducted a user study on real-world videos to evaluate different methods from a subjective perspective. We randomly selected 20 videos from the DAVIS dataset, each with a resolution of 1024×576 , featuring subjects such as people, animals, and various other objects. Since ground truth disparity maps were unavailable, we generated disparity maps using a depth prediction model [44]. Different methods were used to render the videos with the same control parameters. During testing, the videos were presented in random order to avoid bias. As shown in the interface (Fig. 8), participants were asked to select the method that produced the most consistent and aesthetically pleasing bokeh effect.

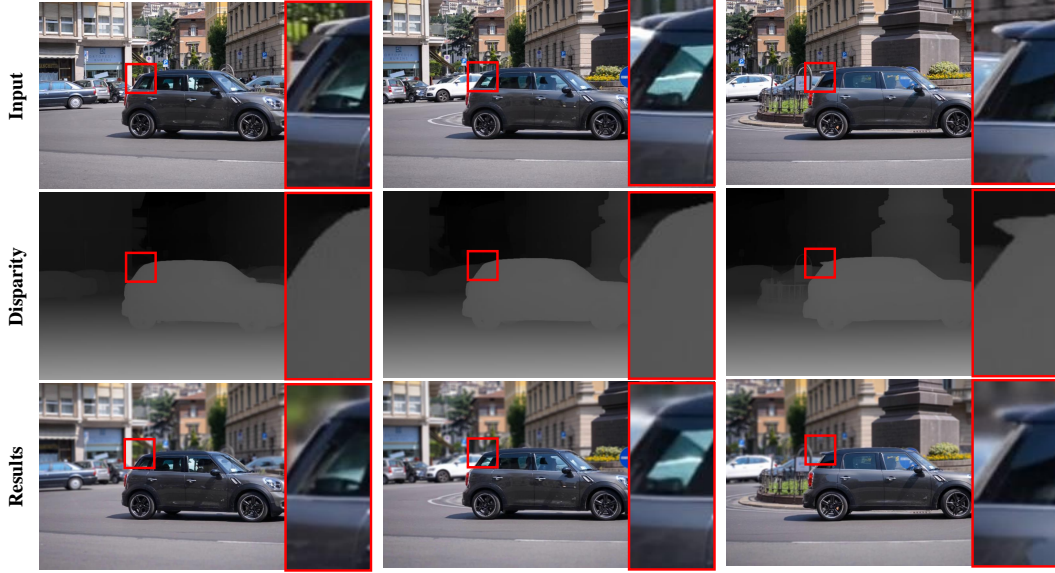


Figure 9: Any-to-Bokeh struggles to recover missing structures in the disparity map.

C Limitations and Future Work

Although our method can handle small differences at the disparity boundaries through temporal consistency, it struggles to recover missing structures in the disparity map due to the significant gap between the training data and real-world scenarios. As shown in Fig. 9, while our method is able to recover part of the missing region in the second frame, the model misidentifies it as the defocus area due to the missing structure in the disparity map. Future work will focus on integrating depth recovery techniques and exploring longer time-series memories to minimize such issues and enhance robustness against severe depth errors.

D More Comparison Results

To further compare the performance of our model with baselines, we selected two representative examples from the DAVIS dataset to demonstrate the superiority of our approach. As shown in Fig. 10, Fig. 11 and Fig. 12, our model produces a more natural bokeh transition at the edges. In contrast, DeepLens struggles with focusing accurately on the correct focal plane due to the limitations of its built-in depth model. Additionally, MPIB, Dr.Bokeh, and BokehMe exhibit varying degrees of edge color bleeding and overly sharp transitions, particularly along hair edges in the images, which leads to an unnatural visual effect. These artifacts underscore the advantages of our method in generating more realistic and visually coherent bokeh effects.

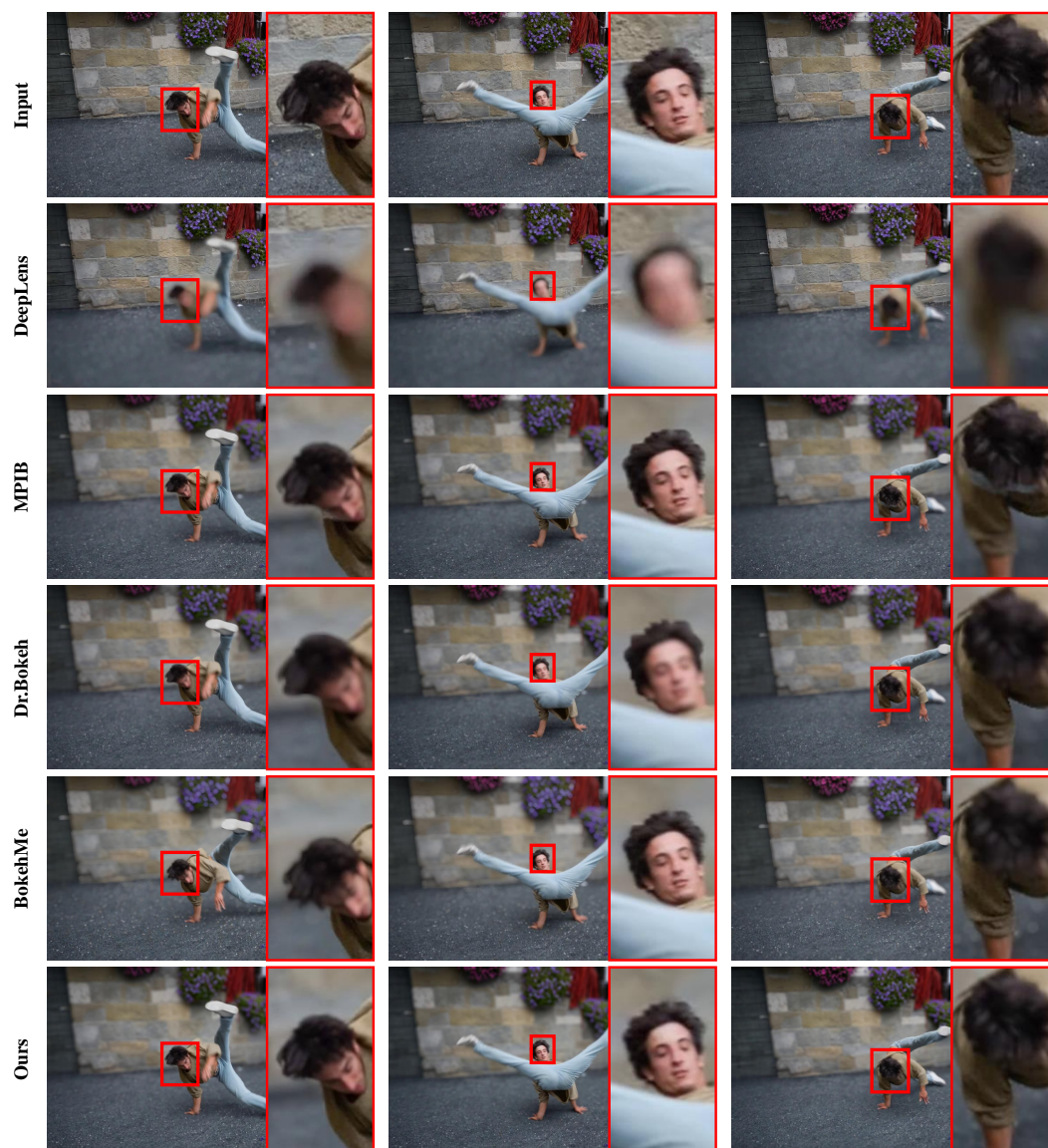


Figure 10: Comparison results with baselines on the real dataset. The area inside the red border is zoomed in to highlight more details. Please zoom in to view them.

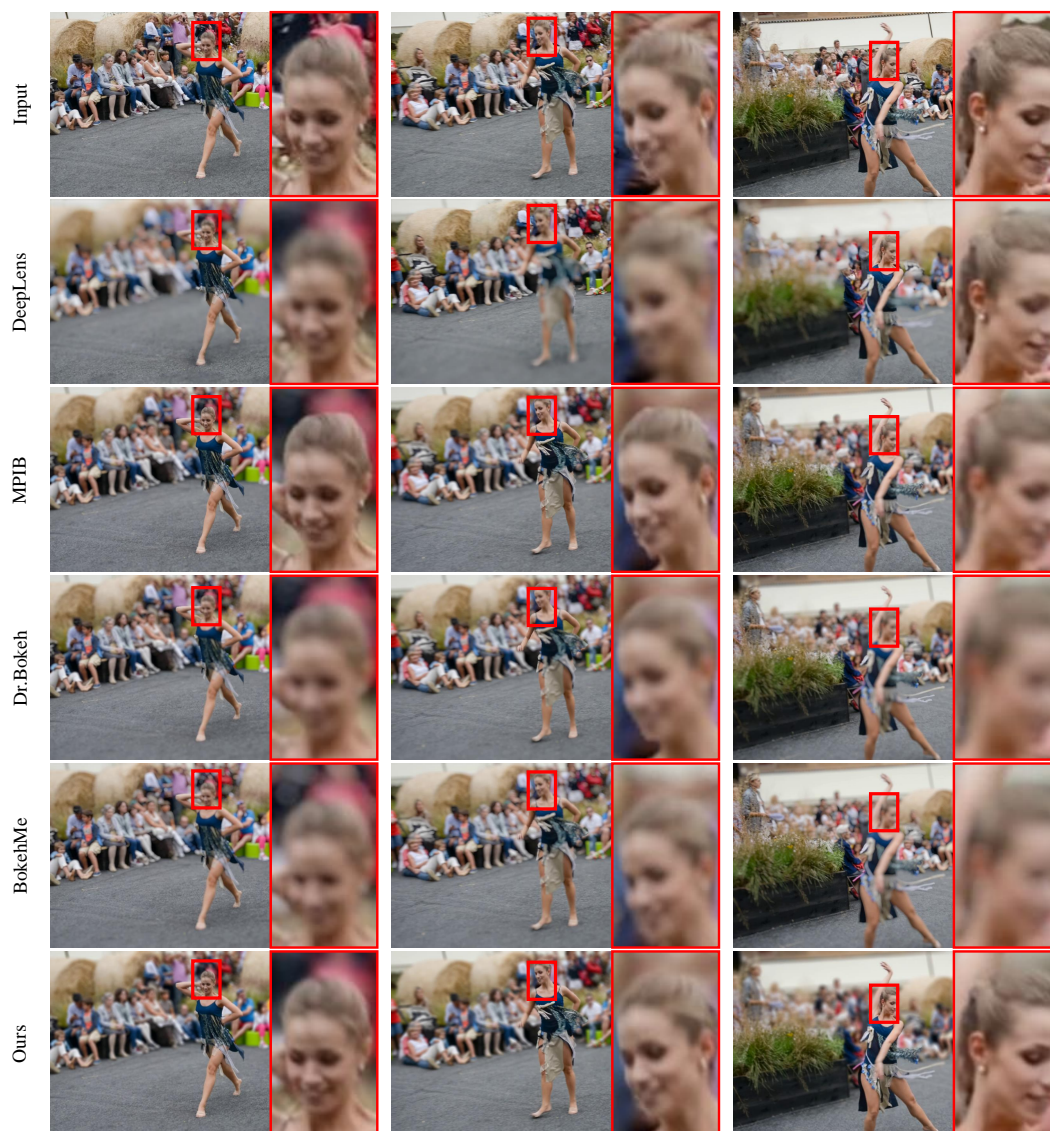


Figure 11: Comparison results with baselines on the real dataset. The area inside the red border is zoomed in to highlight more details. Please zoom in to view them.



Figure 12: Comparison results with baselines on the real dataset. The area inside the red border is zoomed in to highlight more details. Please zoom in to view them.